JOURNAL OF MATERIALS SCIENCE 2 (1967) 339–346

The Distribution of Iron Impurity in Single-Crystal Magnesium Oxide and Some Effects on Mechanical Properties

R. W. DAVIDGE
Ceramics Division, Atomic Energy Research Establishment, Harwell, Berks, UK

Received 14 April 1967

MgO containing $\leqslant$5000 wt ppm Fe was heat-treated in various ways, so that the Fe was present in solution as Fe^{2+} or Fe^{3+}, as precipitates of $MgO.Fe_2O_3$, or as metallic bcc Fe. Crystals were studied by optical absorption spectroscopy and microscopy. Heating in air at 1400° C converts most of the Fe to Fe^{3+} and some of this is associated with vacancies, particularly at high impurity levels. In crystals containing Fe^{3+}, the magnitude of the hardening is relatively about four times less than that in alkali halides containing divalent metallic impurities, where all the impurities are associated with charge-compensating vacancies. Greater hardening is obtained when precipitates of $MgO.Fe_2O_3$ are present. Precipitates of metallic bcc Fe are formed on heating in hydrogen at temperatures >1000° C; these have the orientation relationships $(001)_{MgO} \,||\, (001)_{Fe}$ and $[110]_{MgO} \,||\, [100]_{Fe}$.

1. Introduction

Magnesium oxide/iron oxide mixtures have received much attention in the past in view of their importance to refractories used in steel making [1]. There are also possible electronic applications owing to the presence of ferri- or ferro-magnetic precipitates. Fe is a major impurity in typical, commercial, MgO single crystals, often present in concentrations >100 ppm. The form and distribution of Fe depends critically on the heat-treatment of the crystal and on whether this occurs in a reducing or oxidising atmosphere. Fe can take at least four distinct forms: (i) in substitutional solution as Fe^{2+}; (ii) in substitutional solution as Fe^{3+}; (iii) as precipitates of $MgO.Fe_2O_3$; (iv) as precipitates of metallic Fe.

These forms are investigated here mainly by optical absorption and microscopy, and their effects on the room-temperature flow stress are examined in MgO single crystals containing $\leqslant$5000 ppm Fe.

2. Crystals

Four crystals were used: one from the Norton Co* (N) containing 150 ppm Fe, and three grown from melts deliberately doped with iron oxide (F1, F2, F3) containing 300 to 5000 ppm Fe. Spectrographic analyses are given in table I. It would seem that one incidental advantage of adding Fe is the reduction in the levels of other impurities.

TABLE I Analyses of crystals (wt ppm).

	Detected					Not detected
	Al	Ca	Fe	Mn	Zr	(all crystals)
N	150	50	150	10	8	Ti, V, <50; Co, Cr,
F1	70	300	300	20	1	Si, Zn, <20; Mo,
F2*			1000			<10; Be, Cd, Cu,
F3	30	<10	5000	25	1	Sb, <5; Ni, <2; Bi, In, Pb, Sn, <1; Ga, <0.5; Ge, <0.2

*only analysed for Fe

Specimens were annealed in air or oxygen for the production of Fe^{3+}, in carbon monoxide for Fe^{2+}, and in hydrogen for metallic Fe. At 1400° C, equilibrium is obtained in about 1 day for a specimen 1 mm thick. $MgO.Fe_2O_3$ precipitates

*Worcester, Mass, USA

were formed by subsequent annealing of oxidised crystals at 600 to 900° C. Most of this work is concentrated on crystal F3 so as to minimise any effects of the other impurities.

3. The Forms of Fe in MgO

3.1. Fe in Substitutional Solid Solution

In MgO substitutional solution, Fe can assume at least two valencies: Fe^{2+}, favoured by reducing conditions, and Fe^{3+}, favoured by oxidising conditions; in the latter case, one charge-compensating Mg vacancy must be present for each two Fe^{3+} ions. FeO (equivalent to Fe^{2+} in solution) is completely miscible in MgO [2], whereas Fe_2O_3 (equivalent to Fe^{3+}) is not [3] and, at temperatures $\lesssim 1000°$ C, $MgO.Fe_2O_3$ can precipitate out in the form of octahedra coherent with the MgO matrix [4]. When Fe^{3+} is present, it is therefore necessary to cool crystals rapidly to room temperature to retain the Fe in solution. The $[Fe^{3+}]/[Fe^{2+}]$ ratio produced by a given heat-treatment (above $\sim 1000°$ C) depends on the crystal composition, the temperature, and the atmosphere.

The oxidation of Fe^{2+} to Fe^{3+} in MgO can be regarded in several ways depending on the precise form of the Fe^{3+}. If the Fe^{3+} is unassociated, one can write:

$$Fe^{2+} + \tfrac{1}{4}\,O_2\,(g) = Fe^{3+} + \tfrac{1}{2}\square + \tfrac{1}{2}\,O^{2-} \quad (1)$$

where $\square$ represents a vacant Mg site. This reaction has an equilibrium constant K_1:

$$K_1 = [Fe^{3+}]^{\frac{1}{2}}/[Fe^{2+}]\,(P_{O_2})^{\frac{1}{4}}$$

so that high total-Fe content will favour a low $[Fe^{3+}]/[Fe^{2+}]$ ratio. However, association reactions between Fe^{3+} ions and vacancies may occur to form dimers, trimers, etc. ($Fe^{3+} + \square = Fe^{3+}\square$, $2Fe^{3+} + \square = Fe^{3+}{}_2\square$, etc.). There is some electron-spin-resonance evidence for the existence of dimers [5] with the impurity and vacancy in next nearest-neighbour positions in <100>. The existence of trimers is in accordance with the observed equilibrium behaviour of MgO containing high concentrations (>3 wt %) of Fe [6]. If, for example, the association reaction $2Fe^{3+} + \square = Fe^{3+}{}_2\square$ is complete, one can write the oxidation reaction as:

$$2Fe^{2+} + \tfrac{1}{2}\,O_2\,(g) = Fe^{3+}{}_2\square + O^{2-} \quad (2)$$

Here the equilibrium constant is K_2:

$$K_2 = [Fe^{3+}{}_2\square]/[Fe^{2+}]^2\,(P_{O_2})^{\frac{1}{2}}$$

so that high total-Fe contents favour a high $[Fe^{3+}]/[Fe^{2+}]$ ratio. Since association will be favoured at high Fe concentrations, reaction (1) should predominate in crystals of low Fe content, and more complex reactions in those of high Fe content.

Ideally, one wishes to know the total concentration of Fe^{3+} ions and also the forms in which they occur. Optical absorption spectra provide a useful means of monitoring the concentration of Fe^{3+} ions in solution. The spectra of fully reduced crystals are featureless apart from some absorption in the far ultraviolet. Numerous absorption bands occur in oxidised crystals when Fe^{3+} is present. Spectra for crystal F3, heat-treated in various ways, are shown in fig. 1. Two of the absorption bands in the oxidised crystal, at 2100 and 2850 Å, have been associated with the presence of Fe^{3+} ions in solution [7]. The saturation level of the 2850 Å band, for crystals annealed in air at 1400° C and rapidly cooled to room temperature, increases with increasing Fe concentration. There is an approximately linear relationship, and results are shown in fig. 2. In addition to heat-treatment, the conversion of Fe^{2+} to Fe^{3+} can be achieved by irradiation. Chen and Sibley [8] show that, in crystals first annealed at 1100° C in argon, the saturation level of the 2850 Å band under γ-irradiation is also linearly proportional to the chemically determined Fe concentration; their results are shown in fig. 2 and cover an impurity range up to 2 orders of magnitude less than the present data. The small numerical difference between the two sets of data is complementary to earlier work of Soshea *et al* [7], who found that the saturation level of the 2850 Å band was less after X-irradiation than after oxygen heat-treatment.

As the Fe^{3+} ions can be produced by irradiation at room temperature, where little diffusion can occur, as well as by heat-treatment, it is highly probable that the 2850 Å band is due to single Fe^{3+} ions; this conclusion would also apply to the 2100 Å band, as this always occurs in sympathy with the 2850 Å band. Furthermore, electron-spin-resonance measurements [9] show that, for crystal F1, at least 90% of the Fe^{3+} ions are present as single unassociated ions; the remainder occur as some form of cluster. Measurements at higher Fe contents have not been possible because of the complexity of the resonance spectrum. At low Fe concentrations, therefore, the predominant Fe defects are single Fe^{3+} ions. The linearity between the absorption

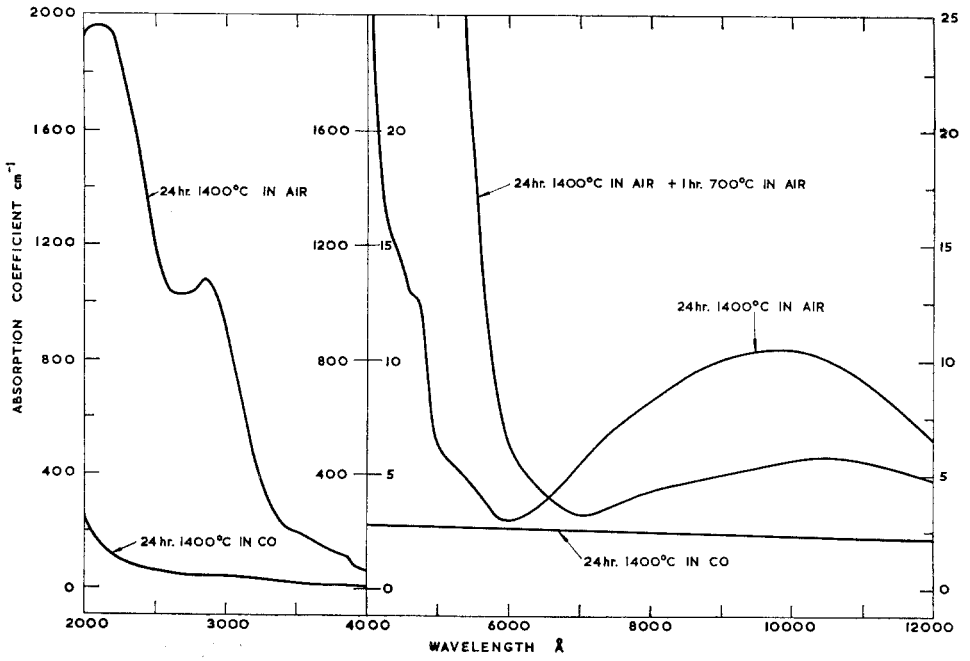

Figure 1 Optical absorption spectra for crystal F3 after three heat-treatments.

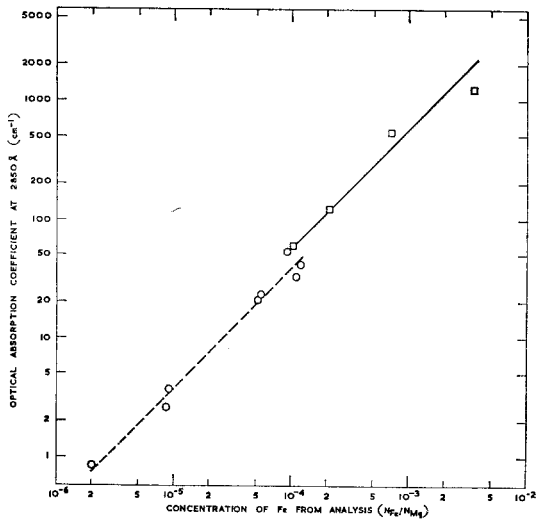

Figure 2 Variation of absorption at 2850 Å with Fe content: — —O— — saturation level on γ-irradiation (Chen and Sibley [8]); ——◇—— saturation level on heating in air at 1400° C.

in the 2850 Å band and the Fe concentration suggests that reaction (1) dominates and that the oxidation process is virtually complete.

Assuming that oxidation to Fe^{3+} is complete, and that the predominant cluster in the more impure crystals is the dimer, one can estimate relative concentrations of unassociated Fe^{3+} ions. For example, if the Fe^{3+} ion/dimer ratio in crystal F1 (300 ppm) is 90/10, the corresponding ratio for crystal F3 (5000 ppm) is ~60/40. Experimentally (fig. 2), about 60% of the Fe in crystal F3 is observed as unassociated Fe^{3+} ions, thus giving support to this idea.

It is possible to obtain an oscillator strength for single Fe^{3+} ions using the formula [10]

$$Nf = 0.87 \times 10^{17}\, n\,(n^2 + 2)^{-2}\,\alpha W$$

where: N is the number of centres per cubic centimetre; f, the oscillator strength of the centre; n, the refractive index; α, the absorption coefficient at the peak wavelength (cm^{-1}); W, the half-width of the absorption band (eV). For crystal F1, $N = 1.2 \times 10^{19}/cm^3$, $n = 1.80$, $\alpha = 120$ cm^{-1}, and $W = 0.70$ eV for the 2850 Å band, so that $f = 0.040$. Thus, for this band, $N = 1.0 \times 10^{17}$ α; this enables direct estimates of $[Fe^{3+}]$ to be made from optical absorption data.

In crystal F3 (fig. 1), other unresolved bands occur in the oxidised crystal on the high wavelength side of the two Fe^{3+} bands. The bands lie at approximately 3600, 3850, 4600, and 5400 Å and are responsible for the yellow coloration of this crystal. The first two of these bands are detectable in the other three crystals in the oxidised state. No assignations for these bands have yet been made. A subsequent heat-treatment of the oxidised crystals at 700° C, in the

precipitation range, causes a large increase in absorption in the lower visible and ultraviolet regions, but without any resolvable bands.

The remaining feature is the broad band in the infrared at ~10 000 Å, which is prominent in the oxidised crystal F3; there is no evidence for this band in the other crystals. The intensity is reduced during a second anneal at 700° C, when precipitation occurs. The band is tentatively assigned to some cluster of Fe^{3+} ions and vacancies.

3.2. $MgO.Fe_2O_3$ Precipitates

Optical evidence of precipitation was found in oxidised specimens of F3 on annealing at 600 to 900° C. These specimens showed a dark-brown coloration (see fig. 1), but without any resolved bands. The morphology of the precipitates has been fully discussed by Groves and Fine [4]. Further evidence of precipitation may be obtained from etching studies, as done previously for a crystal similar to N [11].

3.3. Metallic Fe Precipitates

Specimens from all four crystals are quite colourless after heating in carbon monoxide at ~1400° C and show no detectable signs of precipitation. Specimens from crystals N, F1, and F2 heated in hydrogen are also colourless, but specimens of F3 appear black. Optical microscopy reveals a high density of precipitates in these latter crystals. For crystals viewed normal to (001) planes, three crystallographic types of precipitate are seen (fig. 3): squares

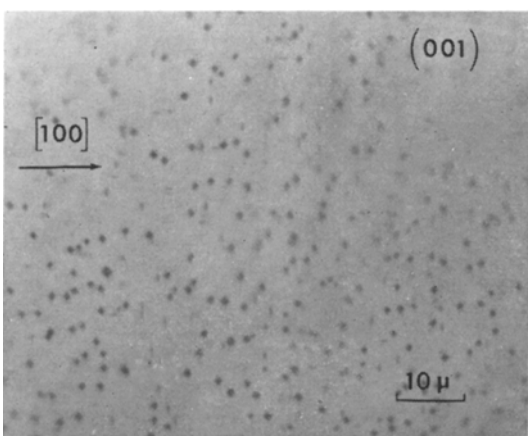

Figure 3 Fe precipitates parallel to the three sets of {100} MgO planes, transmitted light.

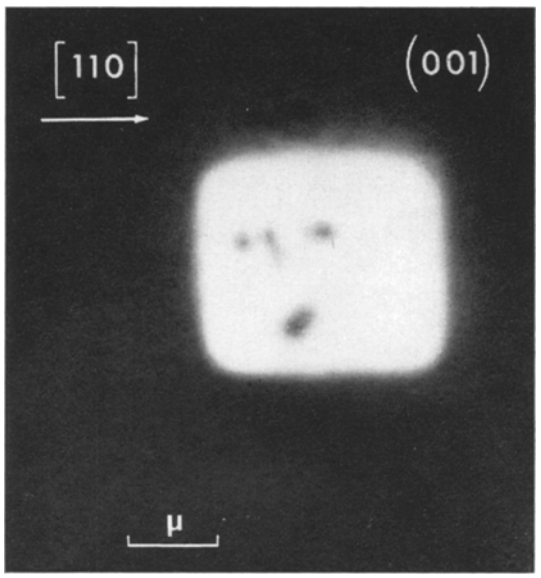

Figure 4 Fe precipitate showing rounded corners and subsidiary faceting, reflected light.

or rectangles with sides parallel to [110] and $[1\bar{1}0]_{MgO}$ and two sets of lines parallel to [100] and $[010]_{MgO}$. This is consistent with the presence of square or rectangular plate-like precipitates in each of the three {100} planes. The precipitates are highly reflecting (fig. 4) and have rounded corners and often subsidiary faceting. Attempts to obtain electron diffraction patterns from the precipitates, by electron microscopy, failed because they were always dissolved out of the thin areas of the specimen during polishing. However, transmission electron micrographs from thicker regions of the specimen show the precipitates to be ~1 μm square and ~0.2 μm thick. The distribution of precipitates is irregular and very high concentrations occur at sub-grain boundaries.

Small pieces of crystal containing precipitates are readily attracted to a magnet, suggesting that Fe in bcc form is present. X-ray diffraction studies of both powdered and single-crystal samples failed to detect Fe. To obtain higher concentrations of precipitates, specimens from crystal N were plated with a layer of powdered Fe metal, ~50 μm thick, and were annealed in air at 1800° C for several hours to diffuse in the Fe. This produced a dark-brown surface layer $\frac{1}{2}$ mm deep. The specimen was then reduced in hydrogen for 1 day at 1300° C. A high density of precipitates formed near the plated surface; these were similar in form,

although less regular in shape than those observed in crystal F3. An X-ray oscillation photograph from this surface showed detectable diffraction due to bcc Fe with the following orientation relationships: $[001]_{MgO} \,||\, [001]_{Fe}$ and $[110]_{MgO} \,||\, [100]_{Fe}$; fig. 5 illustrates this. The two structures have the dimensional relationships:

$$d[110]_{MgO}\ (2.98\ \text{Å}) \simeq d[100]_{Fe}\ (2.87\ \text{Å})$$
$$2d[001]_{MgO}\ (8.42\ \text{Å}) \simeq 3d[001]_{Fe}\ (8.61\ \text{Å})$$

There is very good match between the two (001) planes in these structures.

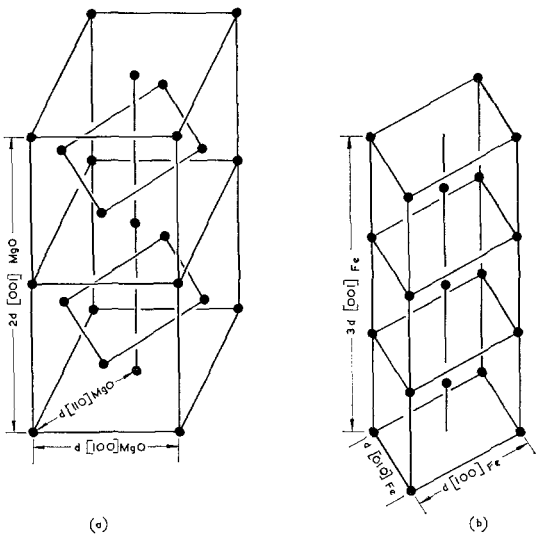

Figure 5 Structural relationship between (a) MgO and (b) bcc Fe (only Mg ions are shown in the MgO lattice).

4. Mechanical Properties of Fe-Doped MgO

Impurities can affect dislocations in two distinct ways: by pinning the existing dislocations or by acting as a lattice resistance to the movement of fresh dislocations. Only the second effect is considered here.

4.1. Measurement of Lattice Resistance

The most direct measurement of lattice hardness is that of the initial flow stress. This is the stress needed to move freshly introduced dislocations through the crystal at a velocity of $\sim 10^{-3}$ cm/sec [12]. A more convenient, although less direct, measurement is that of the indentation wing size [4]. A cleaved surface of the crystal is indented with a microhardness tester and the crystal is etched. The maximum distance that dislocations move away from the indentation can then be measured; this will be greater the softer the crystal. This method has the advantages that many tests can be made on a small sample and that specimens can be subsequently treated, say by annealing, and the hardness then remeasured. According to Groves and Fine [4], the reciprocal of the distance moved by the dislocations from the indenter is roughly proportional to the flow stress of the specimen.

To determine this relationship precisely, a series of flow-stress and indentation-pattern measurements were made on a range of specimens of various hardness. The flow stress was measured in three-point bending for specimens that had first been sprinkled with carborundum powder to introduce fresh dislocations. Microhardness indents were then made using a 30 g load on the same specimens. The indentation wing sizes in $<110>$ directions were measured as indicated in fig. 6. Fig. 7 shows the correlation between flow stress and wing size.

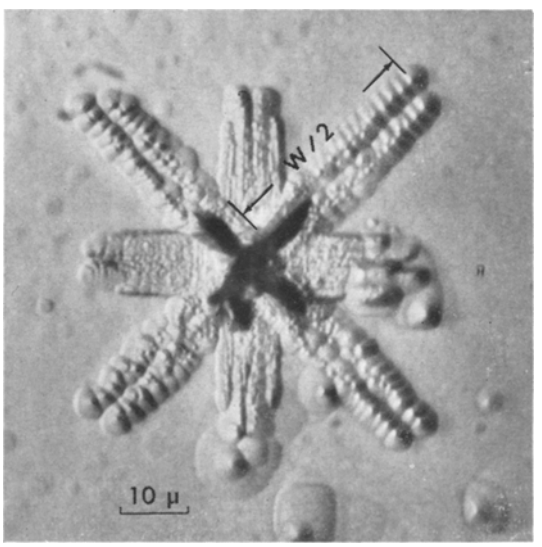

Figure 6 Method of measurement of wing size (W).

Over a wide flow-stress range, there is proportionality between flow stress and reciprocal wing size. There is some deviation at low flow stresses. In what follows, all lattice hardness measurements were made by the indentation method and converted to equivalent flow stresses from fig. 7.

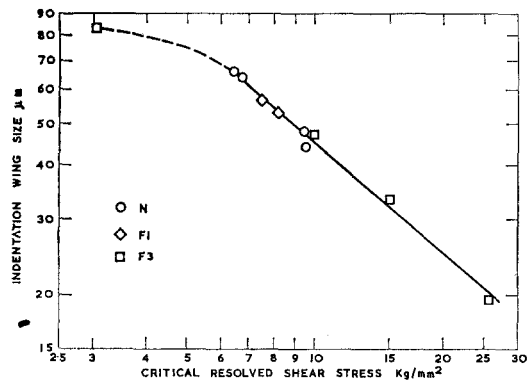

Figure 7 Indentation wing size as a function of critical resolved shear stress (CRSS).

4.2. Effects of Fe on Lattice Hardness

Some values of the flow stress of crystals N, F1, and F3 after various heat-treatments are shown in table II.

TABLE II Values of the room-temperature flow stress (kg/mm²) for N, F1, and F3 after various treatments: (i) reduction; (ii) oxidation; and (iii) oxidation plus precipitation.

Crystal \ Treatment	(i) 1 day, 1400° C in CO, air-cooled	(ii) 1 day, 1400° C in air, air-cooled	(iii) as (ii) + 1 h at 700° C in air
N	5.7	6.4	10.4
F1	4.1	4.3	7.2
F3	3.0	13.0	30.0

The type of atmosphere has little effect for crystals N and F1, which have low Fe concentrations, but for F3 there is a large effect. Similarly, precipitation hardening effects are much greater in F3 than in N or F1. The hardness of F3 is thus readily varied with heat-treatment by an order of magnitude; more detailed results for F3 are presented below. It is convenient to discuss separately the effects of Fe in solution and as precipitates of $MgO.Fe_2O_3$. No measurements were made on crystals containing metallic Fe, since the density of precipitates was low and their distribution non-random.

4.2.1. Solution Effects

Samples of crystal F3, originally treated in carbon monoxide to reduce most of the Fe to Fe^{2+}, were heated in sealed tubes under oxygen pressures <200 torr at 1300° C for 1 day, and were rapidly cooled. The concentrations of single Fe^{3+} ions were obtained from measured absorption coefficients at 2850 Å using the relationship derived in section 3.1. Fig. 8 correlates the Fe^{3+} concentrations (c) with the measured flow stresses

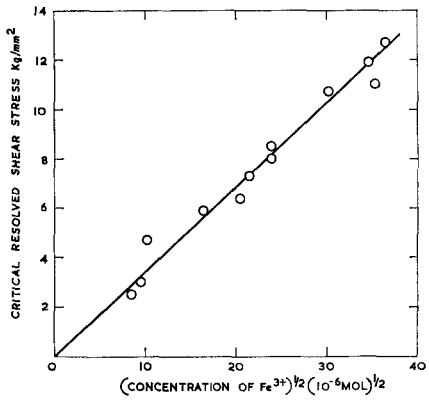

Figure 8 Relationship between CRSS and Fe^{3+} concentration.

(τ); the data fit the relationship $\tau \propto c^{\frac{1}{2}}$. Since the graph passes through the origin, it can be assumed that the intrinsic lattice hardness and the effects of Fe^{2+} ions are small. The implications behind these results are not clear cut, because it has not been possible to monitor all the defects present. Apart from single Fe^{3+} ions, there will also be present charge-compensating vacancies. Both these defects are expected to have only a small elastic interaction with dislocations because of their high symmetry [13, 14]. However, the electronic disturbance introduced by these defects could cause some hardening. In addition, clusters of Fe^{3+} ions and vacancies are also likely, and concentrations of $\sim 40\%$ of dimers may be present. Because of their non-symmetrical strain field, such defects will have a higher hardening rate than the above defects. On this basis, since, according to the reaction $Fe^{3+} + \square = Fe^{3+}\square$, $[Fe^{3+}\square] \propto [Fe^{3+}]^{\frac{1}{2}}$, hardening due to dimers would be of the form $\tau \propto c^{\frac{1}{2}}$ if these were the dominant hardening agents.

These data may be compared with those for the alkali halides, where there is a high degree of association between vacancies and divalent cations. The hardness of MgO shows a temperature-dependence up to $\sim 800°$ K [11], which is about 3 times the temperature range found in the alkali halides. In comparing the two types

TABLE III Effect of impurities on hardness in NaCl, LiF, and MgO.

System	Temperature	CRSS* per 100 ppm† impurity (10^8 dyn/cm^2)	Shear modulus C_{44} (10^{11} dyn/cm^2)	CRSS/C_{44}
NaCl/Ca^{++} [15]	Liquid nitrogen	1.0	1.3	8×10^{-4}
LiF/Mg^{++} [16]	Liquid nitrogen	4.1	6.4	6×10^{-4}
MgO/Fe^{3+}	Room	3.0	14.8	2×10^{-4}

*critical resolved shear stress
†expressed as $N_{\text{impurity}}/N_{\text{cation}}$

of material, it therefore seems appropriate to use the present data at room temperature and that for the alkali halides at liquid-nitrogen temperature (i.e. about 1/10 of the melting temperature in both cases). This is done in table III. Whereas the hardening of NaCl and LiF is similar when expressed in terms of the shear modulus, the hardening in MgO is 3 to 4 times lower, as expected from the lower degree of association. It is not possible at present to determine the separate effects of the various types of defect on the hardness of MgO, although, by analogy with alkali halides, one expects that dimers (or larger aggregates) would have by far the greatest effect.

4.2.2. Precipitation Effects

Isochronal and isothermal hardness curves for crystal F3 are shown in figs. 9 and 10. Similar curves, but with smaller hardness changes,

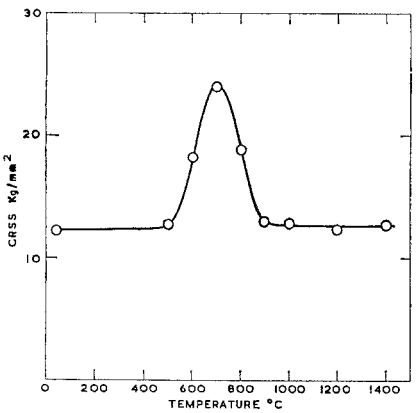

Figure 9 Variation of CRSS of crystal F3, initially containing Fe^{3+}, on successively annealing for 1 h at increasing temperatures.

were found for the other crystals. Each curve was made for single specimens that had originally been annealed at 1400° C in air and rapidly cooled to produce a high concentration of

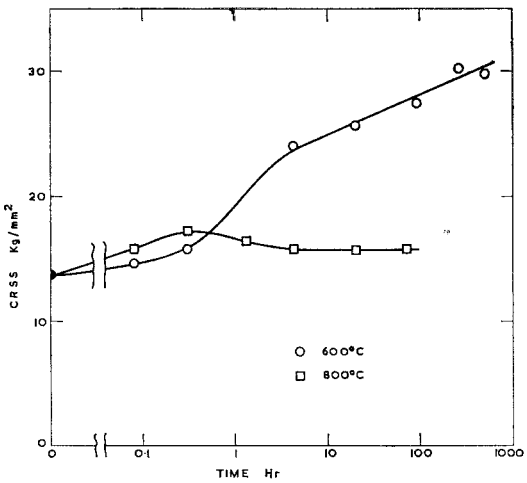

Figure 10 Variation of CRSS of crystal F3, initially containing Fe^{3+}, at 600 and 800° C as a function of time.

Fe^{3+}. Between each hardness measurement, a few microns were chemically polished off the surface of the specimen. The curves show features expected from a precipitation hardening mechanism in agreement with the conclusion of other recent investigations [11, 17]. The magnitude of the hardening is greatest at the lower temperature, where more impurity will precipitate out, but a much longer time is needed to give maximum hardness. At 800° C, maximum hardness is obtained in ~20 min; for longer times, the crystal gets softer owing to over-ageing.

Acknowledgements

Thanks are due to Dr F. J. P. Clarke, Dr B. Henderson, Mr R. D. King, and Dr J. Williams for many helpful discussions throughout the course of this work.

References

1. D. WOODHOUSE and J. WHITE, *Trans. Brit. Ceram. Soc.* **54** (1955) 333.

2. N. L. BOWEN and J. F. SCHAIRER, *Amer. J. Sci.* **29** (1935) 153.
3. B. PHILLIPS, S. SOMIYA, and A. MUAN, *J. Amer. Ceram. Soc.* **44** (1961) 169.
4. G. W. GROVES and M. E. FINE, *J. Appl. Phys.* **35** (1964) 3587.
5. J. E. WERTZ, G. S. SAVILLE, L. HALL, and P. AUZINS, *Proc. Brit. Ceram. Soc.* **1** (1964) 59.
6. J. BRYNESTAD and H. FLOOD, *Z. Elecktrochem.* **62** (1958) 953.
7. R. W. SOSHEA, A. J. DEKKER, and J. P. STURTZ, *J. Phys. Chem. Solids* **5** (1958) 23.
8. Y. CHEN and W. A. SIBLEY, *Phys. Rev.* **154** (1967) 842.
9. B. HENDERSON, Phys. Dept., Keele Univ., Staffs., private communication.
10. D. L. DEXTER, *Sol. State Phys.* **6** (1958) 355.
11. G. D. MILES, F. J. P. CLARKE, B. HENDERSON, and R. D. KING, *Proc. Brit. Ceram. Soc.* **6** (1966) 325.
12. W. G. JOHNSTON and J. J. GILMAN, *J. Appl. Phys.* **30** (1959) 129.
13. R. L. FLEISCHER, *Acta Met.* **10** (1962) 835.
14. *Idem, J. Appl. Phys.* **33** (1962) 3504.
15. R. P. HARRISON, P. L. PRATT, and C. W. A. NEWEY, *Proc. Brit. Ceram. Soc.* **1** (1964) 197.
16. W. G. JOHNSTON, *J. Appl. Phys.* **33** (1962) 2050.
17. R. J. STOKES, *J. Amer. Ceram. Soc.* **48** (1965) 60.